A Distal Tyrosine Residue Is Required for Ligand Discrimination in DevS from *Mycobacterium tuberculosis*[†]

Erik T. Yukl,[‡] Alexandra Ioanoviciu,[§] Michiko M. Nakano,[‡] Paul R. Ortiz de Montellano,[§] and Pierre Moënne-Loccoz*,[‡]

Department of Environmental and Biomolecular Systems, OGI School of Science and Engineering, Oregon Health and Science University, 20000 NW Walker Road, Beaverton, Oregon 97006-8921, and Department of Pharmaceutical Chemistry, University of California, 600 16th Street, San Francisco, California 94158-2517

Received June 30, 2008; Revised Manuscript Received September 18, 2008

ABSTRACT: DevS is a heme-based sensor kinase required for sensing environmental conditions leading to nonreplicating persistence in *Mycobacterium tuberculosis*. Kinase activity is observed when the heme is a ferrous five-coordinate high-spin or six-coordinate low-spin CO or NO complex but is strongly inhibited in the oxy complex. Discrimination between these exogenous ligands has been proposed to depend on a specific hydrogen bond network with bound oxygen. Here we report resonance Raman data and autophosphorylation assays of wild-type and Y171F DevS in various heme complexes. The Y171F mutation eliminates ligand discrimination for CO, NO, and O_2, resulting in equally inactive complexes. In contrast, the ferrous−deoxy Y171F variant exhibits autokinase activity equivalent to that of the wild type. Raman spectra of the oxy complex of Y171F indicate that the environment of the oxy group is significantly altered from that in the wild type. They also suggest that a solvent molecule in the distal pocket substitutes for the Tyr hydroxyl group to act as a poorer hydrogen bond donor to the oxy group. The wild-type CO and NO complexes exist as a major population in which the CO or NO groups are free of hydrogen bonds, while the Y171F mutation results in a mild increase in the distal pocket polarity. The Y171F mutation has no impact on the proximal environment of the heme, and the activity observed with the five-coordinate ferrous−deoxy wild type is conserved in the Y171F variant. Thus, while the absence of an exogenous ligand in the ferrous−deoxy proteins leads to a moderate kinase activity, interactions between Tyr171 and distal diatomic ligands turn the kinase activity on and off. The Y171F mutation disrupts the on−off switch and renders all states with a distal ligand inactive. This mechanistic model is consistent with Tyr171 being required for distal ligand discrimination, but nonessential for autophosphorylation activity.

Mycobacterium tuberculosis (MTB)[1] is believed to have latently infected as many as 2 billion people worldwide (*1*). The success of this pathogen relies in part on its ability to exist within the host in a dormant state known as "nonreplicating persistence" (NRP) for extended periods, with subpopulations phenotypically resistant to current chemotherapies (*2*). Thus, a detailed understanding of NRP and its initiation process is critical for improving the treatment of TB.

NRP is characterized by the induction of a set of 48 genes, the so-called "dormancy regulon". Included in this set is α-crystallin, a heat-shock protein likely involved in the stabilization of essential proteins and cell structures during extended quiescence (*3*). Hypoxia and NO are likely environmental cues prompting entrance into NRP as expression of the dormancy regulon was found to be induced in response to both hypoxia and exposure to nontoxic concentrations of NO (*4*). Furthermore, O_2 was shown to competitively inhibit NO-mediated induction of the dormancy regulon (*4*). These observations strongly suggest that one sensor is responsible for detecting both signals and initiating the expression profile responsible for NRP.

Mutagenesis studies identified the DevR/DevS/DosT system as being required for induction of the dormancy regulon in response to hypoxia and NO (*4, 5*). This is a classical two-component regulatory system where DevR is a response regulator of the LuxR family (*6*) and DevS and its closely related (60% identical, 76% similar) paralog, DosT, are histidine protein kinases (HPK) (*5*) responsible for phosphorylation and activation of DevR.

Both DevS and DosT are modular in nature with an N-terminal sensing core composed of two tandem GAF domains and a C-terminal kinase core with a HisKA (histidine kinase phospho-acceptor) domain where autophos-

[†] This work was supported by Grants GM74785 (P.M.-L.) and AI074824 (P.R.O.d.M.) from the National Institutes of Health.

* To whom correspondence should be addressed. Telephone: (503) 748-1673. Fax: (503) 748-1464. E-mail: ploccoz@ebs.ogi.edu.

[‡] Oregon Health and Science University.

[§] University of California.

[1] Abbreviations: MTB, *Mycobacterium tuberculosis*; NRP, nonreplicating persistence; GAF domain, protein domain conserved in cyclic GMP-specific and stimulated phosphodiesterases, adenylate cyclases, and *Escherichia coli* formate hydrogenlyase transcriptional activator (Pfam accession number PF01590); GAF A and GAF B, first and second N-terminal GAF domains of DevS and DosT, respectively; wt, wild type; Y171F, tyrosine 171 to phenylalanine mutation; IPTG, isopropyl β-D-thiogalactopyranoside; RR, resonance Raman.

10.1021/bi801234w CCC: $40.75
Published on Web 11/01/2008

phorylation occurs and an HATPase (histidine kinase-like ATPase) domain responsible for binding ATP (*7*). The first GAF domain (GAF A) binds heme and acts as a diatomic gas sensor (*7*−*10*). DevS and DosT exhibit autokinase activity when the heme is in the deoxy state, signaling hypoxia, and when NO or CO is bound to the Fe(II) ion (*9*). In contrast, the kinase activity is strongly inhibited by the binding of O_2 (*9*). The ferric state (met) of DevS was also reported to lack autophosphorylation activity (*10*).

Previously, we reported the resonance Raman (RR) characterization of truncated and full-length wt DevS (*11*). The results suggested that a specific hydrogen bond exists between a distal residue and the proximal oxygen atom of bound O_2. This hydrogen bond was absent from CO and NO adducts as well as from the ferrous unligated state. On the basis of this evidence and the apparent function of DevS in vivo, we proposed that this hydrogen bond was responsible for differentiating exogenous ligands and that, when engaged, would inhibit kinase activity. Thus, only the kinase activity of the oxy complex would be inhibited, whereas the Fe(II), NO-, and CO-bound states should be active. These conclusions were confirmed by autophosphorylation experiments (*9, 10*). Moreover, CO sensing during macrophage infection has been shown to result in activation of the dormancy regulon (*12, 13*). The X-ray structure of GAF A of DosT shows that the hydroxyl group of Tyr169 (Tyr171 in DevS) acts as a hydrogen bond donor to oxygen (*14*). Since our experiments indicated stability issues with Y169F DosT, we report on the RR characterization and autokinase activity of the Y171F mutant of DevS in the Fe(III), Fe(II), Fe−CO, Fe−NO, and Fe−O_2 states and compare the results to those of wt DevS. Because the wt Fe−O_2 complex is inactive, and Tyr171 interacts with the bound O_2, the Y171F mutation might have been expected to release inhibitory constraints to produce a Y171F variant equally active in the O_2, NO, and CO complexes. However, our results show that the Y171F variant lacks autokinase activity in all three states where the distal pocket is occupied by an exogenous ligand and retains activity only in the deoxy form. These activity measurements are discussed in conjunction with the RR analysis with the aim of proposing mechanistic models of regulation in DevS.

MATERIALS AND METHODS

Full-Length DevS Mutagenesis. The full-length DevS gene previously cloned into pET23a+ was mutated using Pfu turbo and the following mutagenic primers: CGTTCGGCACTCTGTTCCTGACTGACAAGACC (forward primer) and GGTCTTGTCAGTCAGGAACAGAGTGCCGAACG (reverse primer). DNA sequencing was used to verify the mutated gene sequence.

Y171F DevS Expression. The mutant protein was expressed following the same protocol used in the case of DevS642 (*8*). Briefly, BL21gold DE3 cells were cotransformed with pET23a+ Y171F DevS and pT-GroE, and the cells were grown on LB plates containing both ampicillin (50 μg/mL) and chloramphenicol (34 μg/mL). Starter cultures were grown at 37 °C and then used to inoculate flasks containing 1.5 L of LB medium and the antibiotics ampicillin (100 μg/mL) and chloramphenicol (34 μg/mL). The cells were grown to an optical density (OD_{600}) of 0.8−1 at 37 °C and 230 rpm. Hemin was added before induction (45 mg/1.5 L of culture), and protein expression was induced with IPTG at a final concentration of 1 mM. The cultures were kept at 18 °C for 20 h, and then the cells were harvested by centrifugation at 5000 rpm for 25 min.

Protein Purification. The cells were lysed in phosphate buffer (pH 7.6) [50 mM NaH_2PO_4, 10% glycerol, 200 mM NaCl, 1% Triton X-100, 0.5 mg/mL lysozyme, 5 mM $MgCl_2$, 5 mM ATP, and protease inhibitors antipain (1 μg/mL), leupeptin (1 μM), pepstatin (1 μM), and PMSF (0.1 mM)]. Then the mixture was incubated with shaking at 37 °C for 30 min. The cell membranes were disrupted by repeated sonication cycles at 50% using a Branson model 450 sonifier from VWR Scientific while being cooled on ice. The insoluble fraction was isolated by centrifugation at 35000 rpm for 1 h at 4 °C. The cell lysate was applied to a 5 mL His trap column. The column was washed with 20 and 50 mM imidazole buffer. The recombinant protein was then eluted with 250 mM imidazole. The protein sample was applied to a DEAE column. The purified protein was obtained after gradient elution from 0 to 0.5 M NaCl in 50 mM Tris buffer containing 5% glycerol and 1 mM EDTA at pH 8.

Electronic Absorption and Resonance Raman Spectroscopy. The RR experiments were performed with ~100 μM protein solutions for the Fe(III) and deoxy−Fe(II) forms, and ~300 μM protein solutions for the CO, NO, and O_2 complexes. Ultrafree-0.5 ultrafiltration devices (Millipore) were used for concentrating the protein. A 50 mM potassium phosphate buffer at pH 7.5 with 100 mM NaCl was used for most protein samples; 100 mM MES (pH 6.0), 100 mM potassium phosphate (pH 7.0), 50 mM HEPES (pH 8.0), 200 mM CHES (pH 9.5), and 200 mM CAPS (pH 11.0) were used in pH dependence experiments. Reduction to the ferrous state was achieved by adding aliquots (a few microliters) of a concentrated sodium dithionite solution (35−50 mM) to an argon-purged sample. ^{12}CO (Airgas) and ^{13}CO (99% ^{13}C; ICON Stable Isotopes) adducts were obtained by injecting CO through a septum-sealed capillary containing argon-purged, reduced protein (~20 μL). O_2 (Airgas), $^{18}O_2$ (99% ^{18}O; ICON Stable Isotopes), NO (Aldrich), and $^{15}N^{18}O$ (98% ^{15}N and 95%^{18}O; Aldrich) adducts were generated using the same procedure after excess dithionite was removed from the reduced sample with desalting spin columns (Zeba 0.5 mL; Pierce). These procedures were performed in a glovebox with a controlled atmosphere of <1 ppm O_2 (Omni-Laboratory System, Vacuum Atmospheres Co.). All samples were monitored by UV−vis spectroscopy directly in the capillary using a Cary 50 spectrophotometer (Varian). RR spectra were obtained using a custom McPherson 2061/207 spectrograph (0.67 m with variable gratings) equipped with a Princeton Instruments liquid N_2-cooled CCD detector (LN-1100PB). Kaiser Optical supernotch filters or long-wave pass filters (RazorEdge Raman filters, Semrock) were used to attenuate Raleigh scattering. A krypton laser (Innova 302, Coherent) and a He/Cd laser (Liconix 4240NB) were used for 413 and 442 nm excitations, respectively. Spectra were collected in a 90° scattering geometry on samples at room temperature. Frequencies were calibrated relative to indene and CCl_4 and are accurate to ±1 cm^{-1}. CCl_4 was also used to check the polarization conditions. The integrity of the RR

samples, before and after laser illumination, was confirmed by direct monitoring of their UV−vis spectra in the Raman capillaries.

Autophosphorylation Assays. wt or Y171F DevS protein solutions in 50 mM potassium phosphate buffer (pH 7.5) with 100 mM NaCl were purged with Ar and reduced with sodium dithionite. Excess dithionite was removed using desalting columns, and CO, NO, or O_2 gas was added to appropriate samples. The Fe(III) proteins were incubated in 2 mM potassium ferricyanide and desalted using spin columns. These operations were performed in the anaerobic glovebox. All samples, except the oxy and Fe(III) proteins, were loaded into septum-sealed microcentrifuge tubes. All 50 μL assay samples contained final concentrations of 5.0 μM DevS, 100 mM Tris-HCl (pH 7.5), 50 mM KCl, 5 mM $MgCl_2$, and, with the exception of oxy and Fe(III) samples, 500 μM sodium dithionite, after ATP addition. Reactions were initiated by syringe addition of a few microliters of a solution containing [γ-^{32}P]ATP (4500 Ci/mmol) (Pharmacia Biotech) and Ar-purged, unlabeled ATP (Sigma) to a final concentration of 200 μM and 10 μCi. Aliquots (10 μL) were removed at various time points and combined with 3.0 μL of stop buffer [208 mM Tris-HCl (pH 6.8), 8.3% SDS, 42% glycerol, 167 mM DTT, and 0.08% bromophenol blue]. These samples were run through a 12% polyacrylamide gel, which was vacuum-dried at 80 °C for 1.5 h, and exposed in a PhosphorImager cassette (Molecular Dynamics) for approximately 24−48 h. Levels of phosphorylated protein were imaged on a Typhoon Trio+ PhosphorImager (Amersham Biosciences) and quantified according to the method of Nakamura et al. (*15*), except that the correction factor of 1.65 was eliminated since gels were completely dried. After exposure, dried gels were rehydrated in a 20% methanol/5% acetic acid solution and Coomassie stained to confirm consistency in the amount of protein loaded and the integrity of full-length proteins.

RESULTS

Autokinase Activity of wt and Y171F DevS. Autophosphorylation assays were performed by monitoring γ-^{32}P labeling of DevS for 10 min at room temperature (Figure 1). Different states of wt DevS exhibited autokinase activities consistent with a previous report by Gilles-Gonzalez and coworkers (*9*). However, in our hands, the ferrous protein is systematically less active than the nitrosyl complex, while equivalent activities are reported for these two states by Sousa et al. (*9*). Indeed, multiple experiments with two different wt DevS constructs yielded the same pattern of activity for the various states of DevS (Figure S1 of the Supporting Information). Mutation of Tyr171 to Phe has no apparent impact on the autophosphorylation level observed in the Fe(II) state, but the mutation disrupts the discriminatory power of DevS toward exogenous ligands with the CO-, NO-, and O_2-bound states all lacking activity (Figure 1). As reported previously for wt DevS (*10*), the met Fe(III) state of Y171F is inactive (Figure S2 of the Supporting Information). These data are consistent with a determining role for the hydroxyl group of Tyr171 in distinguishing between distal exogenous ligands in DevS. The maintenance of autophosphorylation activity in the deoxy form of Y171F DevS demonstrates that the point mutation does not result in a major protein conformational change. In the deoxy form, the heme is pentacoordinate (see below) and the lack of a distal ligand results in a lack of sensitivity to the Tyr171 to Phe mutation.

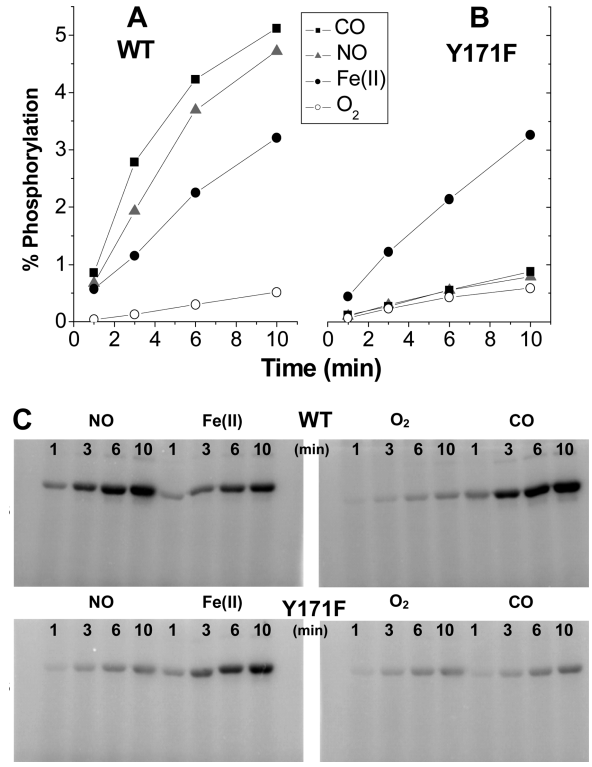

FIGURE 1: (A and B) Time courses for the autophosphorylation of wt (A) and Y171F (B) DevS in the Fe(II) (●), Fe(II)−CO (■), Fe(II)−NO (▲), and Fe(II)−O_2 (○) forms. (C) Autoradiographs of the dried gels for wt DevS (top) and Y171F DevS (bottom).

Table 1: UV−Vis Spectroscopic Data for wt and Y171F DevS

DevS protein	Soret and visible λ_{max} (nm)
Fe(III) wt	406, 500, 630
Fe(III) Y171F	409, 540, 633
Fe(II) wt	428, 562
Fe(II) Y171F	429, 561
Fe(II)−CO wt	422, 570, 540
Fe(II)−CO Y171F	421, 569, 540
Fe(II)−NO wt	419, 577, 547
Fe(II)−NO Y171F	419, 573, 544
Fe(II)−O_2 wt	414, 578, 543
Fe(II)−O_2 Y171F	420, 573, 542

Spectroscopic Analysis of wt and Y171F DevS. UV−vis spectroscopic data for wt and Y171F DevS at pH 7.5 are summarized in Table 1. Distinctive absorption features were obtained for the Fe(II), Fe−CO, and Fe−NO forms, with both proteins exhibiting nearly identical spectra. The Fe(III) form of Y171F shows significant red shifts in the α/β region, a decrease in intensity of the charge transfer band near 630 nm, and a red shift and a significant decrease in the extinction coefficient of the Soret band (Table 1 and Figure S3 of the Supporting Information). These observations suggest an increase in the proportion of low-spin Fe(III) heme in the mutant relative to wt protein (*16*). This interpretation of the UV−vis changes is consistent with the high-frequency RR spectra obtained with Soret excitation (Figure 2) in which the frequency of the porphyrin skeletal mode ν_4 correlates with the oxidation state of the iron and those of the ν_3, ν_2, and ν_{10} modes report the coordination and spin state of the

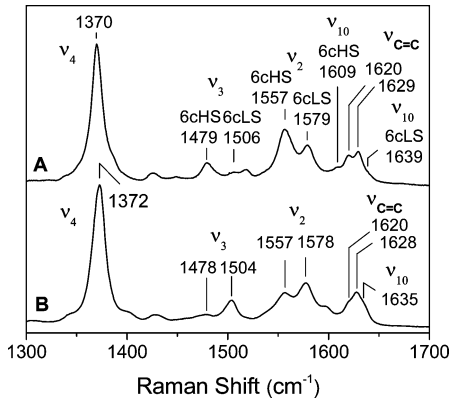

FIGURE 2: High-frequency RR spectra of ferric wt DevS (A) and Y171F DevS (B) at room temperature (λ_{exc} = 413 nm; 5 mW).

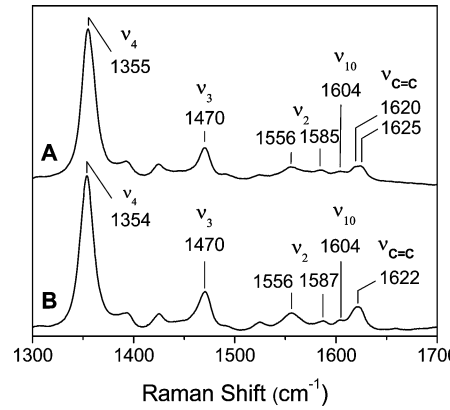

FIGURE 3: High-frequency RR spectra of ferrous deoxy wt DevS (A) and Y171F DevS (B) at room temperature (λ_{exc} = 413 nm; 5 mW).

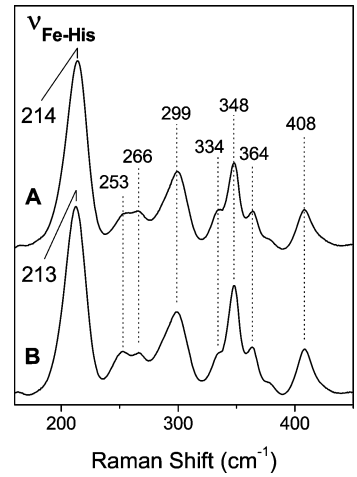

FIGURE 4: Low-frequency RR spectra of ferrous deoxy wt DevS (A) and Y171F DevS (B) at room temperature (λ_{exc} = 442 nm; 10 mW).

iron (*17*). Specifically, in the wt, the ν_3, ν_2, and ν_{10} modes observed at 1479, 1557, and 1609 cm^{-1}, respectively, are indicative of a six-coordinate high-spin (6cHS) heme, while those at 1506, 1579, and 1639 cm^{-1}, respectively, correspond to a six-coordinate low-spin (6cLS) population (Figure 2A). Equivalent sets of frequencies are also observed in the RR spectrum of the Y171F variant (Figure 2B and Table 2), but the relative intensities of these bands suggest a shift in the 6cHS−6cLS distribution, from predominantly 6cHS in the wt protein to predominantly 6cLS in the variant protein.

RR spectra of ferric wt and Y171F DevS at different pH values show that conversion from high-spin to low-spin ferric heme occurs at a much lower pH in Y171F (pH ~7) than it does in wt DevS (pH ~10) (Figure S4 of the Supporting Information). These observations suggest that the removal of the hydroxyl group of Tyr171 alters the ligand field strength of the distal ligand. At pH 10, the Tyr171 side chain may coordinate the wt heme Fe(III) as a phenolate ligand. Alternatively, a solvent molecule may coordinate the heme Fe(III) with a bond strength that is governed by its interaction with Tyr171. In the Y171F DevS variant, the sixth ligation to the Fe(III) is most likely occupied by a solvent molecule with a pK_a near 7. Attempts to gather direct evidence identifying the sixth ligand in ferric wt and Y171F DevS were unsuccessful. Specifically, low-frequency RR spectra in $^{18}OH_2$ and D_2O did not reveal isotope-sensitive modes that could be assigned to a ν(Fe−OH) mode, as previously observed with hydroxy complexes in heme oxygenases and hemoglobin at high pH (*18*−*21*), or to a ν(Fe−O_{Tyr}) as previously observed in the 6cLS alkaline ferric *Chlamydomonas* hemoglobin (*22*) (Figure S5 of the Supporting Information).

The high-frequency RR spectra of Fe(II) wt and Y171F DevS are both indicative of a pure five-coordinate high-spin (5cHS) heme (Figure 3 and Table 2). Two ν(C═C) vinyl stretches are observed in wt DevS at 1620 and 1625 cm^{-1}, but a single broad ν(C═C) stretch is observed at 1622 cm^{-1} in Y171F DevS. A similar perturbation is seen in the Fe(III) state, where two well-resolved ν(C═C) vibrations are observed at 1620 and 1629 cm^{-1} in the wt protein, while the Y171F variant shows a dominant ν(C═C) stretch at 1628 cm^{-1} and a shoulder at 1620 cm^{-1} (Figure 2). Although these data indicate a slight difference in the vinyl groups in the wt and variant proteins, the equivalent activity of the Fe(II) state in these two proteins suggests that the vinyl perturbations have little impact on function. The low-frequency RR spectrum of wt DevS protein, obtained wiht 442 nm excitation (Figure 4), exhibits a strong band at 214 cm^{-1},

Table 2: Resonance Raman Frequencies (cm^{-1}) for wt and Y171F DevS in Various Heme States (minor spectral components in parentheses)

DevS protein	heme state	ν_4, ν_3, ν_2, ν_{10}	$\nu_{C=C}$	δ_{CCC}	ν_{Fe-L}	$\nu_{(X-O)}$
Fe(III) wt	6cHS (6cLS)	1370, 1479, 1557, 1609 (1372, 1506, 1579, 1639)	1620, 1629	370, 385		
Fe(III) Y171F	(6cHS) 6cLS	(nd, 1478, 1557, nd) 1372, 1504, 1578, 1635	1628, 1620 sh	375, 388		
Fe(II) wt	5cHS	1355, 1470, 1556, 1604	1620, 1625	348, 364	214 ν_{Fe-His}	
Fe(II) Y171F	5cHS	1354, 1470, 1556, 1604	1622 broad	348, 364	213 ν_{Fe-His}	
Fe(II)−CO wt	6cLS	1372, 1495, 1580, nd	1625	379, 387	490 (524)	1971 (1936)
Fe(II)−CO Y171F	6cLS	1372, 1496, 1582, nd	1626	379, 387	497	1965
Fe(II)-O_2 wt	6cLS	1374, 1503, 1578, 1636	1629	375, 385	563	no
Fe(II)−O_2 Y171F	6cLS	1373, 1500, 1578, 1633	1627	375, 385	567	no
Fe(II)−NO wt	6cLS	1374, 1498, 1576, nd	1626	378, 385	561	1638 (1604)
Fe(II)−NO Y171F	6cLS	1375, 1499, 1579, nd	1627	378, 385	564	1635

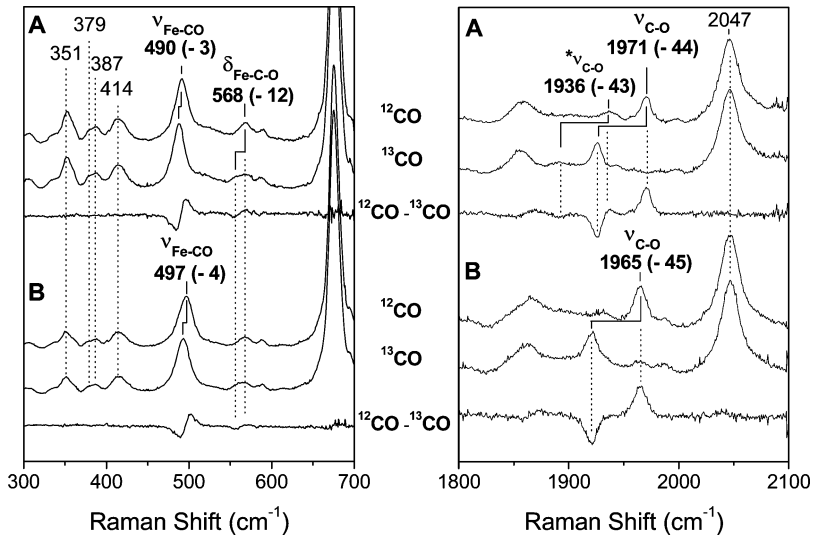

FIGURE 5: Low- and high-frequency RR spectra of the ^{12}CO and ^{13}CO complexes of wt DevS (A) and Y171F DevS (B) at room temperature (λ_{exc} = 413 nm; <0.5 mW). ^{12}CO − ^{13}CO difference spectra are also shown; the asterisk indicates contributions from a minor CO conformer (*11*).

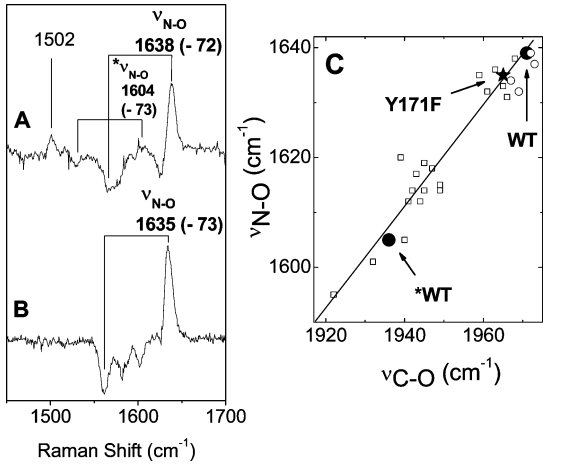

FIGURE 6: (A and B) High-frequency RR $^{14}N^{16}O$ − $^{15}N^{18}O$ difference spectra of wt DevS (A) and Y171F DevS (B) (λ_{exc} = 413 nm; 0.5 mW). The asterisk indicates contributions from a minor NO conformer (*11*). (C) ν(N−O) vs ν(C−O) plot of heme nitrosyl and carbonyl complexes with proximal His ligation for wt DevS (●, with an asterisk for the minor comformers), Y171F DevS (★), wt and distal variants of myoglobin (□), and other heme sensor proteins (○) (see refs *11* and *31* and references therein).

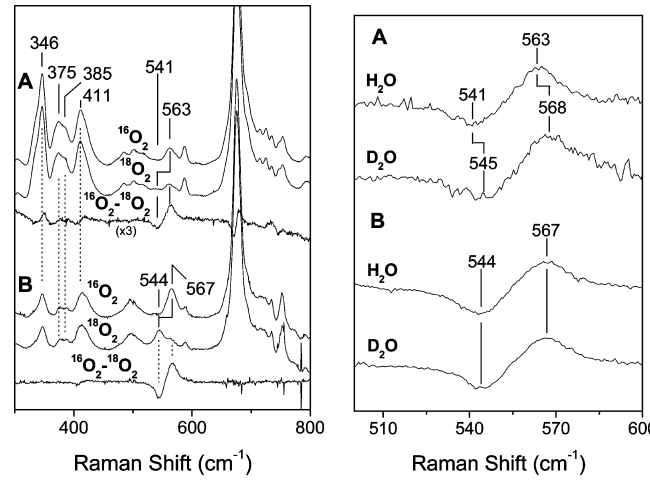

FIGURE 7: (Left) Low-frequency RR spectra of wt (A) and Y171F (B) DevS − $^{16}O_2$, DevS − $^{18}O_2$, and $^{16}O_2$ − $^{18}O_2$ difference spectra. (Right) Low-frequency $^{16}O_2$ − $^{18}O_2$ difference spectra[2] of wt DevS in H_2O and D_2O (A) and of Y171F DevS in H_2O and D_2O (B) at room temperature (λ_{exc} = 413 nm; 0.5 mW).

previously assigned to the ν(Fe−N_{His}) mode (*8*). This mode shifts −1 cm^{-1} in the RR spectrum of Y171F DevS, while other low-frequency heme peripheral deformation modes are nearly identical in both proteins (Figure 4). These results indicate that the effect of the Y171F mutation is limited to the distal environment and does not significantly perturb the proximal heme pocket of DevS.

RR spectra of wt and Y171F DevS−^{12}CO and −^{13}CO complexes are shown in Figure 5. The RR spectrum of wt DevS shows a major CO conformer with ν(C−O) at 1971 cm^{-1} and ν(Fe−CO) at 490 cm^{-1} (*11*). These ν(C−O) and ν(Fe−CO) frequencies are characteristic of a heme−CO complex with a neutral proximal histidine and a carbonyl group free of hydrogen bond interactions in a hydrophobic environment (*11, 23*). Our previous work with truncated DevS proteins consisting of the single GAF A and the two GAF domains (*11*) suggested the presence, in full-length DevS, of a second very minor CO conformer, with ν(C−O) and ν(Fe−CO) bands at 1936 and 524 cm^{-1}, respectively, that is engaged in electrostatic and/or hydrogen bond interactions within the distal pocket. The RR spectra of the CO complex of the Y171F mutant exhibit a ν(C−O) at 1965 cm^{-1} and a ν(Fe−CO) at 497 cm^{-1} (Figure 5). The variations in ν(C−O) and ν(Fe−CO) frequencies in the two proteins suggest only a modest change in the degree of back-bonding from the filled Fe d orbital to the empty π^* orbital of the bound CO in the variant compared to the wt protein. A δ(Fe−C−O) near 568 cm^{-1} is observed with equivalent intensity and ^{13}C shift (−12 cm^{-1}) in both proteins (Figure 5). Finally, the Y171F mutation does not appear to affect interactions of the heme propionate groups since the 350−450 cm^{-1} regions of the RR spectra are equivalent in wt and Y171F DevS (Figure 5). The $\delta(C_\beta C_c C_d)$ propionate deformation modes are sensitive to electrostatic interactions at the heme propionate groups (*24*) and are tentatively assigned to bands at 379 and 387 cm^{-1} (Table 2).

Comparison of the high-frequency $^{14}N^{16}O$ − $^{15}N^{18}O$ difference spectra of wt and Y171F DevS leads to an analysis

similar to that for the CO data (Figure 6). As discussed previously (*11*), vibrational mixing between $\nu(^{15}N-^{18}O)$ and vinyl $\nu(C=C)$ and ν_2 modes (*25*) increases the number of differential signals contributing to these traces. Despite these perturbations, the strongest positive band in the $^{14}N^{16}O - {}^{15}N^{18}O$ difference spectra is readily assigned to $\nu(^{14}N-^{16}O)$, and it is observed at 1638 and 1635 cm^{-1} in wt and Y171F DevS, respectively (Figure 6). Moreover, the values for the major $\nu(N-O)$ and $\nu(C-O)$ bands in wt and Y171F DevS closely follow the linear correlation observed for other heme proteins sharing proximal histidine ligation (*26*) (Figure 6C). The minor conformer evidenced by a $\nu(N-O)$ at 1604 cm^{-1} in the wt protein (*11*) is not observed in the Y171F variant. Overall, both NO and CO complexes exhibit a modest increase in the level of back-bonding in Y171F DevS relative to the major conformer of the wt protein. As with the carbonyl complex, the low-frequency RR spectra of the nitrosyl adduct show very little difference between wt and Y171F [see the $\nu(Fe-NO)$ and $\delta(C_\beta C_c C_d)$ frequencies in Table 2].

As anticipated on the basis of the crystal structure of DosT, the oxy complexes of wt and Y171F DevS show greater divergence than do any other states of these proteins, illustrating that Tyr169 (DosT numbering) directly interacts with the heme-bound oxygen group (*14*). The Soret absorbance of the variant is red-shifted 6 nm relative to that of the wt protein (Table 1 and Figure S6 of the Supporting Information). Porphyrin skeletal modes ν_4 and ν_3 in the RR spectra show 1 and 3 cm^{-1} downshifts, respectively, in the variant protein relative to the wt protein (Figure S7 of the Supporting Information and Table 2). The $\nu(Fe-O_2)$ mode is isolated from porphyrin modes in the low-frequency RR spectra using $^{16}O_2 - {}^{18}O_2$ difference spectra (Figure 7) and was previously observed in wt DevS at 563 cm^{-1} with a 22 cm^{-1} ^{18}O downshift (*11*). In Y171F, the $\nu(Fe-O_2)$ mode is observed at 567 cm^{-1}, i.e., 4 cm^{-1} higher than in the wt oxy complex. We have previously shown that H−D exchange affects the $\nu(Fe-O_2)$ mode of wt DevS with an ~4 cm^{-1} upshift of the $^{16}O_2 - {}^{18}O_2$ differential signal in D_2O (Figure 7) (*11*). No such effect is observed in Y171F (Figure 7), reflecting a perturbation of hydrogen bonding to the proximal oxygen atom of bound O_2 in this mutant (*27*). As seen with the carbonyl and nitrosyl complexes, mutation of Tyr171 had no significant impact on the frequency of the $\delta(C_\beta C_c C_d)$ propionate deformation modes in the oxy complexes (Figure 7 and Table 2).

DISCUSSION

The crystal structure of GAF A DosT identifies Tyr169 as the sole polar side chain in the distal pocket and as the hydrogen bond partner to the metal-bound O_2 in the oxy form of the protein (*14*). A sequence alignment comparison of DosT and DevS predicts that, in DevS, the Tyr171 hydroxyl group is a hydrogen bond donor to the oxy group in the O_2 adduct, as well as in the minor population of hydrogen-bonded CO and NO conformers identified in the RR spectra of the wt protein. The RR spectra of Y171F DevS reported here support this hypothesis since these hydrogen-bonded CO and NO conformers are not observed. In addition, the Y171F mutation significantly lowers the pH at which the ferric heme is converted from high-spin to low-spin. An earlier RR characterization of the ferric wt and His149Ala proximal variant suggested weak coordination of a distal residue as a sixth ligand to the heme Fe(III) (*8*). In view of the crystal structure of GAF A DosT (*14*), it is tempting to propose that in ferric DevS, the Tyr171 OH group interacts with the ferric heme distal ligation site via the intermediate of a solvent molecule and that the ionization of Tyr171 at pH ~10 converts the ferric heme to a six-coordinate low-spin species. The absence of the hydroxyl group in the Y171F variant would allow for stabilization of a solvent molecule as a sixth ligand with a pK_a value similar to those observed in globin ferric−aqua complexes such as myoglobins (pK_a ~ 9.0) and heme oxygenases (pK_a ~ 8.0) (*19, 21, 28*−*30*). We could not confirm this hypothesis with the observation of a $\nu(Fe-OH)$ stretch in the RR spectra of the ferric Y171F variant at alkaline pH, presumably because of conformational disorder. However, coordination of the heme Fe(III) in Y171F by a solvent molecule is consistent with the overall data, including those obtained on the reduced protein. Indeed, stretching modes from the CO and NO adducts in Y171F DevS are only marginally changed from their dominant counterparts in the wt protein and rule out a purely hydrophobic distal environment in the Y171F variant. Electrostatic effects from a solvent molecule on the CO and NO groups would account for the slightly lower $\nu(C-O)$ and $\nu(N-O)$ frequencies observed in Y171F relative to the wt major conformers. In the oxy complex, the variant protein exhibits a $\nu(Fe-O)$ mode at 567 cm^{-1}, which suggests a polar environment and a hydrogen-bond interaction with a solvent molecule rather than the stronger Tyr171 hydrogen bond donor present in the wt protein (*27*).

Autophosphorylation assays of wt and Y171F variant DevS in different heme states demonstrate the crucial role of Tyr171 in ligand discrimination. Mutagenesis of Tyr171 to a nonpolar residue leads to the inability of DevS to distinguish between the exogenous ligands CO or NO and O_2 and leaves all Fe(II)−XO (where X is O, N, or C) complexes inactive. In contrast, the Y171F mutation has no significant impact on the activity of the deoxy−ferrous protein. Because the ferrous hemes of wt and variant DevS are five-coordinate species with a vacant Fe(II) distal ligation site, a conserved level of autophosphorylation activity in the distal variant ferrous protein is not unexpected. Our data also indicate that the autokinase activity in ferrous wt DevS is lower than that of the CO and NO complexes. From these observations, we propose that interactions between Tyr171 and distal diatomic ligands turn the kinase activity on or off, and that the absence of an exogenous distal ligand interacting with Tyr171 leads to an intermediate level of kinase activity. Mutation of Tyr171 to Phe disrupts the on−off switch, leading to an inactive kinase in all states with distal coordination, while the variant retains the intermediate-level kinase activity associated with the empty distal pocket. Many molecular models can be envisioned within this context, but we can delineate several important features.

[2] For both proteins, the solvent H−D exchange was performed by dilution/reconcentration cycles in D_2O (99.9% D, Aldrich) to reach enrichment >80%. The $^{16}O_2 - {}^{18}O_2$ difference spectra were obtained after the RR spectra were normalized on the intense porphyrin ν_7 at 676 cm^{-1}, and the trace for wt DevS was multiplied by a factor 3 to facilitate comparison with that of Y171F DevS. This difference in $I_{\nu_7}/I_{\nu(Fe-O_2)}$ is likely to reflect a greater resonance enhancement of the $\nu(Fe-O_2)$ mode in Y171F than in wt DevS.

(1) The off state is dependent on a hydrogen-bond interaction between the coordinating O atom of the oxy group and the hydroxyl group of Tyr171. This specific hydrogen bond may lock the phenol side chain in an inhibitory conformation which cannot be achieved with NO or CO. In the ferric protein, which is also inhibited (*10*), the Fe(III) sixth coordination site is occupied by a water molecule, and on the basis of the crystal structure of GAF A of DosT (*14*), it is hydrogen bonded by Tyr171. Thus, Tyr171 adopts an equivalent conformation in the ferric and oxy forms of wt DevS.

(2) The on state in the CO and NO complexes requires a hydrogen-bond network that involves Tyr171 and that is distinct from that in the oxy form. Although minor populations of NO and CO conformers interact with Tyr171 via a hydrogen bond, the majority of the CO and NO complexes do not (*11*), and as such, this larger population may release constraints on Tyr171 to allow its hydroxyl group to engage other hydrogen-bond partners in forming the on state. Alternatively, the hydrogen-bonded NO and CO conformers may be the species responsible for the on state, but the hydrogen-bond acceptor is the noncoordinating oxygen atom of the XO group rather than the coordinating atom as in the oxy complex. In either case, the Y171F mutation prevents the formation of the hydrogen-bond network necessary for stabilization of the on state.

(3) The intermediate-level kinase activity observed with the deoxy form of wt DevS is unaffected by the Tyr171 to Phe mutation. The lack of a distal ligand is expected to reduce steric constraints in the distal pocket, and whether the Tyr171 hydroxyl group is present or not, both on and off states may be populated to produce an intermediate-level autokinase activity.

SUPPORTING INFORMATION AVAILABLE

Autophosphorylation assays of two wt DevS constructs and of the ferric form of Y171F DevS and UV−vis and RR spectra of the ferric and oxy forms of wt and Y171F DevS. This material is available free of charge via the Internet at http://pubs.acs.org.

REFERENCES

1. World Health Organization (2006) *Global tuberculosis control: Surveillance, planning, financing*.
2. Dick, T. (2001) Dormant tubercle bacilli: The key to more effective TB chemotherapy? *J. Antimicrob. Chemother. 47*, 117–118.
3. Cunningham, A. F., and Spreadbury, C. L. (1998) Mycobacterial stationary phase induced by low oxygen tension: Cell wall thickening and localization of the 16-kilodalton α-crystallin homolog. *J. Bacteriol. 180*, 801–808.
4. Voskuil, M. I., Schnappinger, D., Visconti, K. C., Harrell, M. I., Dolganov, G. M., Sherman, D. R., and Schoolnik, G. K. (2003) Inhibition of respiration by nitric oxide induces a *Mycobacterium tuberculosis* dormancy program. *J. Exp. Med. 198*, 705–713.
5. Roberts, D. M., Liao, R. P., Wisedchaisri, G., Hol, W. G., and Sherman, D. R. (2004) Two sensor kinases contribute to the hypoxic response of *Mycobacterium tuberculosis*. *J. Biol. Chem. 279*, 23082–23087.
6. Dasgupta, N., Kapur, V., Singh, K. K., Das, T. K., Sachdeva, S., Jyothisri, K., and Tyagi, J. S. (2000) Characterization of a two-component system, devR-devS, of *Mycobacterium tuberculosis*. *Tuberc. Lung Dis. 80*, 141–159.
7. Sardiwal, S., Kendall, S. L., Movahedzadeh, F., Rison, S. C., Stoker, N. G., and Djordjevic, S. (2005) A GAF domain in the hypoxia/NO-inducible *Mycobacterium tuberculosis* DosS protein binds haem. *J. Mol. Biol. 353*, 929–936.
8. Ioanoviciu, A., Yukl, E. T., Moënne-Loccoz, P., and Ortiz de Montellano, P. R. (2007) DevS, a heme-containing two-component oxygen sensor of *Mycobacterium tuberculosis*. *Biochemistry 46*, 4250–4260.
9. Sousa, E. H., Tuckerman, J. R., Gonzalez, G., and Gilles-Gonzalez, M. A. (2007) DosT and DevS are oxygen-switched kinases in *Mycobacterium tuberculosis*. *Protein Sci. 16*, 1708–1719.
10. Kumar, A., Toledo, J. C., Patel, R. P., Lancaster, J. R., Jr., and Steyn, A. J. C. (2007) *Mycobacterium tuberculosis* DosS is a redox sensor and DosT is a hypoxia sensor. *Proc. Natl. Acad. Sci. U.S.A. 104*, 11568–11573.
11. Yukl, E. T., Ioanoviciu, A., Ortiz de Montellano, P. R., and Moënne-Loccoz, P. (2007) Interdomain interactions within the two-component heme-based sensor DevS from *Mycobacterium tuberculosis*. *Biochemistry 46*, 9728–9736.
12. Shiloh, M. U., Manzanillo, P., and Cox, J. S. (2008) *Mycobacterium tuberculosis* senses host-derived carbon monoxide during macrophage infection. *Cell Host Microbe 3*, 323–330.
13. Kumar, A., Deshane, J. S., Crossman, D. K., Bolisetty, S., Yan, B.-S., Kramnik, I., Agarwal, A., and Steyn, A. J. C. (2008) Heme oxygenase-1-derived carbon monoxide induces the *Mycobacterium tuberculosis* dormancy regulon. *J. Biol. Chem. 283*, 18032–18039.
14. Podust, L. M., Ioanoviciu, A., and Ortiz de Montellano, P. R. (2008) 2.3 Å X-ray structure of the heme-bound GAF domain of sensory histidine kinase DosT of *Mycobacterium tuberculosis*. *Biochemistry* (in press).
15. Nakamura, H., Saito, K., and Shiro, Y. (2001) Quantitative measurement of radioactive phosphorylated proteins in wet polyacrylamide gels. *Anal. Biochem. 294*, 187–188.
16. Makinen, M. W., and Churg, A. K. (1983) in *Iron Porphyrins* (Lever, A. B. P., and Gray, H. B., Eds.) pp 141−236, Addison-Wesley Publishing Co., Reading, MA.
17. Spiro, T. G., and Li, X. Y. (1988) in *Biological Applications of Raman Spectroscopy. Vol. 3. Resonance Raman spectra of hemes and metalloproteins* (Spiro, T. G., Ed.) pp 1−37, John Wiley & Sons, New York.
18. Wilks, A., Black, S. M., Miller, W. L., and Ortiz de Montellano, P. R. (1995) Expression and characterization of truncated human heme oxygenase (hHO-1) and a fusion protein of hHO-1 with human cytochrome P450 reductase. *Biochemistry 34*, 4421–4427.
19. Takahashi, S., Wang, J., Rousseau, D. L., Ishikawa, K., Yoshida, T., Takeuchi, N., and Ikeda-Saito, M. (1994) Heme-heme oxygenase complex: structure and properties of the catalytic site from resonance Raman scattering. *Biochemistry 33*, 5531–5538.
20. Kim, D., Yukl, E. T., Moënne-Loccoz, P., and Montellano, P. R. (2006) Fungal heme oxygenases: Functional expression and characterization of Hmx1 from *Saccharomyces cerevisiae* and CaHmx1 from *Candida albicans*. *Biochemistry 45*, 14772–14780.
21. Asher, S. A., Vickery, L. E., Schuster, T. M., and Sauer, K. (1977) Resonance Raman spectra of methemoglobin derivatives. Selective enhancement of axial ligand vibrations and lack of an effect of inositol hexaphosphate. *Biochemistry 16*, 5849–5856.
22. Das, T. K., Couture, M., Lee, H. C., Peisach, J., Rousseau, D. L., Wittenberg, B. A., Wittenberg, J. B., and Guertin, M. (1999) Identification of the ligands to the ferric heme of *Chlamydomonas* chloroplast hemoglobin: Evidence for ligation of tyrosine-63 (B10) to the heme. *Biochemistry 38*, 15360–15368.
23. Ray, G. B., Li, X.-Y., Ibers, J. A., Sessler, J. L., and Spiro, T. G. (1994) How far can proteins bend the FeCO unit? Distal polar and steric effects in heme proteins and models. *J. Am. Chem. Soc. 116*, 162–176.
24. Uchida, T., and Kitagawa, T. (2005) Mechanism for transduction of the ligand-binding signal in heme-based gas sensory proteins revealed by resonance Raman spectroscopy. *Acc. Chem. Res. 38*, 662–670.
25. Tomita, T., Hirota, S., Ogura, T., Olson, J. S., and Kitagawa, T. (1999) Resonance Raman investigation of Fe-N-O structure of nitrosylheme in myoglobin and its mutants. *J. Phys. Chem. B 103*, 7044–7054.
26. Coyle, C. M., Vogel, K. M., Rush, T. S., III, Kozlowski, P. M., Williams, R., Spiro, T. G., Dou, Y., Ikeda-Saito, M., Olson, J. S., and Zgierski, M. Z. (2003) FeNO structure in distal pocket mutants of myoglobin based on resonance Raman spectroscopy. *Biochemistry 42*, 4896–4903.
27. Ohta, T., Yoshimura, H., Yoshioka, S., Aono, S., and Kitagawa, T. (2004) Oxygen-sensing mechanism of HemAT from *Bacillus subtilis*: A resonance Raman spectroscopic study. *J. Am. Chem. Soc. 126*, 15000–15001.

28. Wilks, A., and Moënne-Loccoz, P. (2000) Identification of the proximal ligand His-20 in heme oxygenase (Hmu O) from *Corynebacterium diphtheriae*. Oxidative cleavage of the heme macrocycle does not require the proximal histidine. *J. Biol. Chem. 275*, 11686–11692.
29. Sun, J., Wilks, A., Ortiz de Montellano, P. R., and Loehr, T. M. (1993) Resonance Raman and EPR spectroscopic studies on heme-heme oxygenase complexes. *Biochemistry 32*, 14151–14157.
30. George, P., and Hanania, G. I. (1957) The ionization of acidic metmyoglobin: Ionic-strength charge effects. *Biochem. J. 65*, 756–760.
31. Tomita, T., Gonzalez, G., Chang, A. L., Ikeda-Saito, M., and Gilles-Gonzalez, M. A. (2002) A comparative resonance Raman analysis of heme-binding PAS domains: Heme iron coordination structures of the BjFixL, AxPDEA1, EcDos, and MtDos proteins. *Biochemistry 41*, 4819–4826.

BI801234W